Article:
Jegede, OE, Haque, N, Mullis, AM et al. (2021) Thermal transitions in metastable Cu – 68.5 at. % Co alloy. Canadian Journal of Chemistry. ISSN: 0008-4042

https://doi.org/10.1139/cjc-2021-0228

Thermal transitions in metastable Cu – 68.5 at. % Co alloy.

Oluwatoyin E. Jegede [a*], Nafisul Haque [a,b,] , Andrew M. Mullis [a] and Robert F. Cochrane [a]

[a] School of Chemical & Process Engineering, University of Leeds, Leeds LS2 9JT, UK.

[b] Department of Metallurgical Engineering, NEDUET, University Road, Karachi 75270, Pakistan

*Corresponding author: Oluwatoyin E. Jegede (email: pmoej@leeds.ac.uk)

Arc melted and drop tube processed Cu – 68.5 at. % Co alloy has been subjected to differential thermal analysis (DTA). The liquidus temperature determined from the DTA curves in the arc melt sample (1664 K) was found to be close to phase diagram estimate of 1662 K. In contrast as a result of liquid phase separation in the drop tube samples, the values obtained in the powders were much lower mainly because the compositions of the demixed phases vary from that of the parent melt. The liquidus temperature of the 850 $^{+}$ μm powders was 1632 K while that of the < 38 μm sieve size powder was 1616 K. This variance is due to the asymmetric nature of the metastable phase diagram of the system.

Keywords: Liquid phase separation, Monotectic solidification, Differential thermal analysis (DTA), Drop tube, metastable alloys.

Introduction

One of the most studied immiscible alloy systems with a metastable miscibility gap is the binary Cu-Co alloy system. Over the years the metastable miscibility gap (MG) in the alloy system has been subject of intense interest as liquid phase separation (LPS) is only possible when the alloy is undercooled into the miscibility gap where it separates into L_1 (Co – rich) and L_2 (Cu – rich) liquid phases different from the parent melt [1–5]. The accepted phase diagram of the system has a slightly symmetrical MG with critical composition of 53 at. % Cu and was observed by Cao et al. [6] in their differential thermal analysis (DTA) and glass fluxing experiments on alloys in the composition range 16 – 87.2 at. % Co. The undercooling at which LPS occurred at their critical composition was placed at 1547 K which was 108 K below the equilibrium liquidus. However, Nakagawa [7] and Robinson et al. [8] observed a perfectly symmetrical MG in the system. Cao et al.[1] places the critical undercooling of the equi – atomic composition at 90 K below the equilibrium whereas 80 K was recorded by Robinson et al. [8] who also confirmed that the peritectic temperature of the system (T_p) was 1385 K. Yamauchi et al. [3] however places the value of the critical undercooling at 96 K below the liquidus with a T_p of 1360 K. The details of the MG by Robinson et al. [8] were said to be in agreement to the asymmetrical MG determined from composition analysis of quenched samples by Munitz and Abbaschian [2]. Critical composition values of 58.5 at. % Cu with corresponding temperature of 1556 K has also been cited in literature [9].

A number of microstructural morphologies have been reported in the alloy of varying compositions; dendrites [2,10], dual structures (dendritic and LPS) [11,12] and LPS [1,10,13–16]. In drop tube processed samples, Cao et al. [11] observed that solidification morphology depended on the degree of undercooling. Large droplets with lower cooling rates and undercooling were

characterized by α – cobalt dendrites with well-defined arm spacing while smaller droplets were characterized by uniformly dispersed spherical particles evidence of LPS in these droplets. Core shell microstructures have also been reported in the alloy of composition 68.5 at. % Co alloy processed in a drop tube [5]. These structures were said to be the resultant of the interplay of interfacial energies and temperature and or composition gradient leading to Marangoni motion of dispersed particles of the minority phase formed close to the surface of the parent droplets. Details of the mechanism of formation and characteristics of these microstructures in drop tube processed Cu-Co alloys are given in [5,17].

LPS is highly desirable in the system as with other immiscible alloy systems due to the various LPS patterns formed by their metastable phases enabling their specific design for wide area of specialization [18]. Clearly, undercooling is a pre – requisite for LPS to occur in the Cu – Co alloy system and to a great extent influences its non – equilibrium solidification process as the demixed liquids have different undercooling to each other and to the parent melt thereby following different solidification path on the metastable phase diagram. It is difficult to determine undercooling in drop tube experiments however, this has been inferred from the cooling rate which can be estimated from the diameter of free falling droplets obtained in drop tube experiments using balance of heat fluxes within the droplet using the equation below as described in [19].

$$\dot{T} = \frac{6}{\rho_m C^{pm} D}\left[h_d(T^D - T^R) + \varepsilon\sigma_{SB}(T_D^4 - T_R^4)\right] \qquad (1)$$

Where ρ_m and C_{pm} is the density and specific heat capacity of the alloy melt, h_d, is the heat transfer coefficient of the droplet falling through the gas, D is the droplet diameter, T_D and T_R is

droplet temperature during free fall and room/ ambient temperature respectively, ε is the total surface emissivity and σ_{SB} is the Stefan – Boltzmann's constant.

Differential thermal analysis (DTA) has been used to study different compositions of the Cu-Co alloy. Jegede et al. [20] studied the equi-atomic composition (Cu- 50at. % Co) and found that rapid cooling of the arc melt process was sufficient to cool into the MG and therefore initiate LPS in arc melt samples. Their phase diagram prediction of minimal undercooling requirement for an alloy of equi-atomic composition to access the binodal and spinodal curves [5] was also confirmed in the drop tube samples. They were able to show that the melting temperature of the Co-rich phase varied with cobalt content while that of the Cu-rich phase was approximately 1295 K. The propensity for LPS in the Cu-Co alloy is said to be greatly affected by deviation from the equi-atomic composition due to the shape of the MG in the system [5]. Cao et al. [1] confirmed this in their DTA study of a Cu-rich composition of the alloy (Cu- 32at. % Co) where they found that a considerable amount of undercooling is required for their alloy to access the binodal curve and even higher cooling rate to get to the spinode.

In this article, DTA is used to study a Co-rich composition (Cu- 68.5at. % Co) which is an alloy on the other end of the two alloys discussed above. The aim is to gain insights into the accuracy of the calculated metastable phase diagram of the Co – Cu alloy system determined in a previous study [5] as well as to understand the liquid phase separation behavior and the thermal phase transformations in arc melted and drop tube processed Cu -68.5at. % Co alloy.

Experimental methods

The Cu – 68.5 at. % Co master alloy was prepared from high purity elemental constituents (Co Alfa Aesar 99.998 %; Cu Alfa Aesar 99.999 %) by alloying in an arc melting furnace under a protective argon environment. In order to ensure homogeneity of the ingot, the melt process was repeated nine times. The drop tube experiment was carried out in a 6.5 m drop tube facility having a nitrogen environment. Slices from the ingot were melted in the crucible of the drop tube furnace and the super-heated melt was injected into the drop tube under pressure and this dispersed into varying size droplets which rapidly solidified during free fall down the tube. The solidified powders were collected upon cooling and sieved into different sieve size fractions. A detailed description of the experimental procedure is available elsewhere [5].

Due to the limited amount of powder samples gotten from the drop tube experiment, the size fractions that gave the most powder were considered for the DTA experiment. The DTA measurements were taken using a PerkinElmer™ STA 8000 simultaneous thermal analyzer at heating and cooling rates of 15 $Kmin^{-1}$. Measurements were taken using 52.320 mg of arc melt sample, 23.081 mg and 18.903 mg of the 850 $^{+}$ μm and < 38 μm sieve size fraction of the drop tube powders respectively. Only the DTA curve of the first heating and cooling cycle were considered in this study as the DTA samples showed signs of Cu oxide contamination evidenced by their black appearance and this is thought to be the origin of some of the peaks observed in the second process cycle. Also, it is reasoned that DTA curves from the second cycle upwards are not likely to be representative of the starting material composition. Baseline artefacts were identified on the DTA curves but were not discussed as they are not part of the transformation details of the alloy but of the reference sample. These were subsequently subtracted from all the curves.

All samples were subsequently processed using standard and quantitative metallographic procedures and were examined using a Carl Zeiss Evo MA 15 SEM in backscattered electron mode. Composition of the samples was determined using energy dispersive X-ray spectrometer (EDS) attached to the SEM.

Results and discussion

Fig. 1 is the metastable phase diagram of the alloy system which was obtained by super imposing calculated miscibility gap [5] on the equilibrium phase diagram of the Co – Cu system. The estimated T_p on the diagram (1367 K) was lower to that quoted for the phase diagrams by Cao et al. [6] and Robinson et al. [8] which was 1385 K but not far off from that reported by Yamauchi et al. [3] who reported T_p of 1360 K. The liquidus temperature of the Cu – 68.5 at. % Co alloy is estimated to be 1662 K with the binodal and spinodal decomposition estimated to occur at undercooling of 143 K and 256 K below the liquidus respectively [5]. An alloy on the opposite end of the phase diagram (Co – 68 at. % Cu) has been shown to have liquidus temperature of 1643 K with critical undercooling of 263 K to cool into the binodal region [1]. These estimates suggest the likelihood of liquid phase separation in the alloy in the binodal region rather than in the spinodal region due to the higher degree of undercooling required to access the spinodal curve.

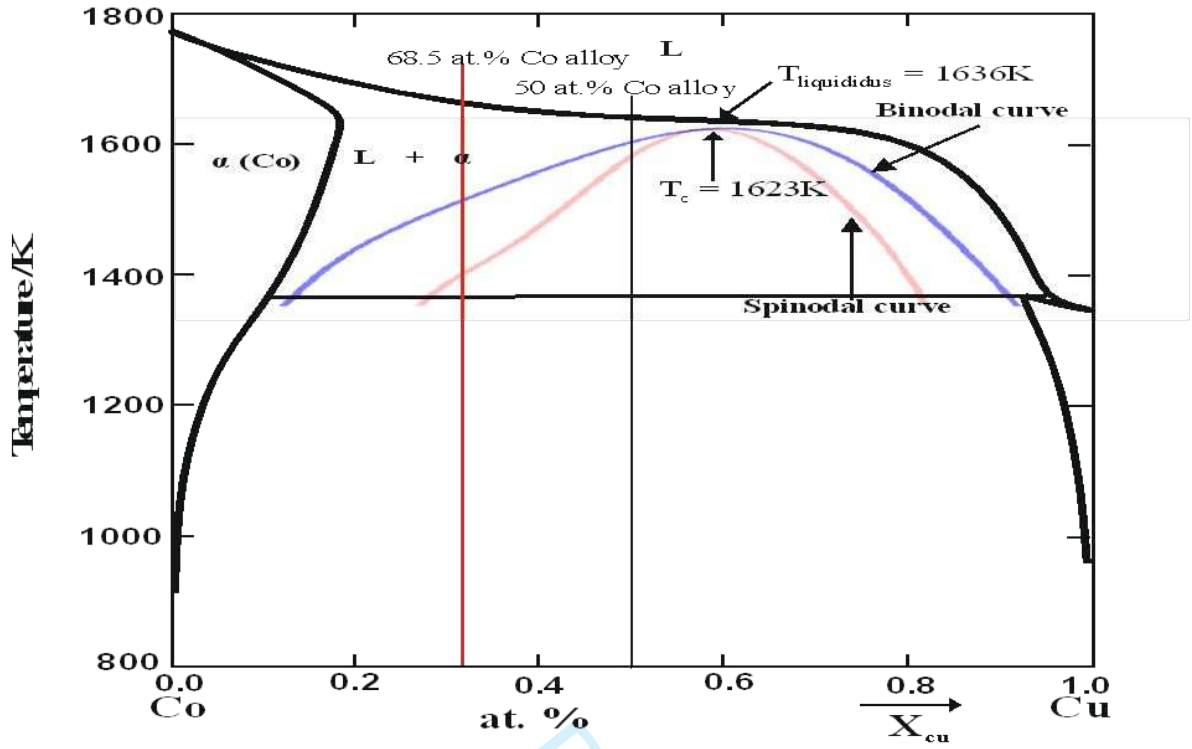

Fig. 1. Metastable phase diagram of the Cu-Co alloy system with calculated miscibility gap showing the binodal and spinodal curves. The solidification path of the Cu 68.5 at. % Co alloy and that of alloy of equi – atomic composition is indicated by the red and black lines respectively [5].

Fig. 2 is a plot of the cooling rate as a function of droplet diameter for the drop tube powders.

Properties for the gas and alloy melt used for the calculation are listed in table 1.

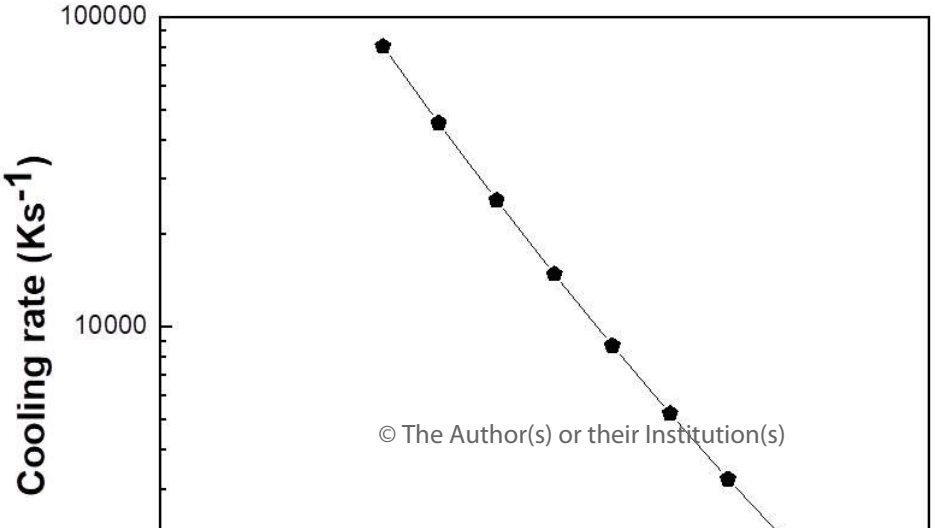

Fig. 2. Estimated cooling rate as a function of droplet diameter in Cu – 68.5 at. % Co alloy.

The figure shows that the calculated cooling rate increases as the droplet diameter decreases with a droplet of diameter 850 µm having a cooling rate of 8.5 x 10^2 Ks^{-1} whereas a 150 µm droplet has an estimated cooling rate of 8.8 x 10^3 Ks^{-1} and a 38 µm droplet is shown to have a cooling rate of 8.1 x 10^4 Ks^{-1}. The translation of this on the solidified microstructures based on phase diagram estimates is that the smaller droplets with the higher cooling rates are able to be sufficiently undercooled into the MG and undergo metastable LPS. However, based on Fig. 1 it is unlikely that the Cu – 68.5 at. % Co alloy would be able to access the spinodal region of the MG as the estimated undercooling required to do so is quite high.

Table 1: Physical properties of gas and alloy melt.

Parameter	Unit	Value
Specific heat capacity (Cg)	J Kg^{-1} K^{-1}	1039
Thermal conductivity (λg)	W m^{-1} K^{-1}	2.4 X 10^{-2}
Dynamic viscosity (µg)	N s m^{-2}	1.76 X 10^{-5}
Prandt number (Pr)		0.7619
Specific heat capacity (C_m)	J Kg^{-1} K^{-1}	590 [a](50% Co)
Specific heat capacity (C_m)	J Kg^{-1} K^{-1}	627 [a](68.5% Co)
Density of melt (ρ_m)	Kg m^{-3}	7885 [a](50% Co)
Density of melt (ρ_m)	,Kg m^{-3}	7835 [a](68.5% Co)
Latent heat of melting (L)	J Kg^{-1}	0
Emissivity of melt (ε)		0.3007 [a]

Stefan Boltzmann constant (σ_B)	W m^{-2} K^{-4}	5.67 X 10^{-8}

[a]Calculated from the pure element based on their atomic fractions.

The microstructure of the arc melt sample is shown below in Fig. 3. As expected from the equilibrium phase diagram of the system, the microstructure observed was dendritic and no evidence of liquid phase separation was seen in the sample. Average dendritic composition determined by EDS (Fig. 4) was 84.27 at. % Co. This is in contrast to the microstructure of the arc melt sample of the equi-atomic composition in which dark spherical particles dispersed in a light matrix was observed, an indication of LPS [20]. This variance is believed to be as a result of the slightly higher estimated cooling rate for the equi-atomic alloy. The higher the cooling rate, the greater the degree of undercooling therefore it was possible for the Cu-50at. % Co alloy to access the MG much faster than the Cu-68.5at. % Co alloy during the solidification process.

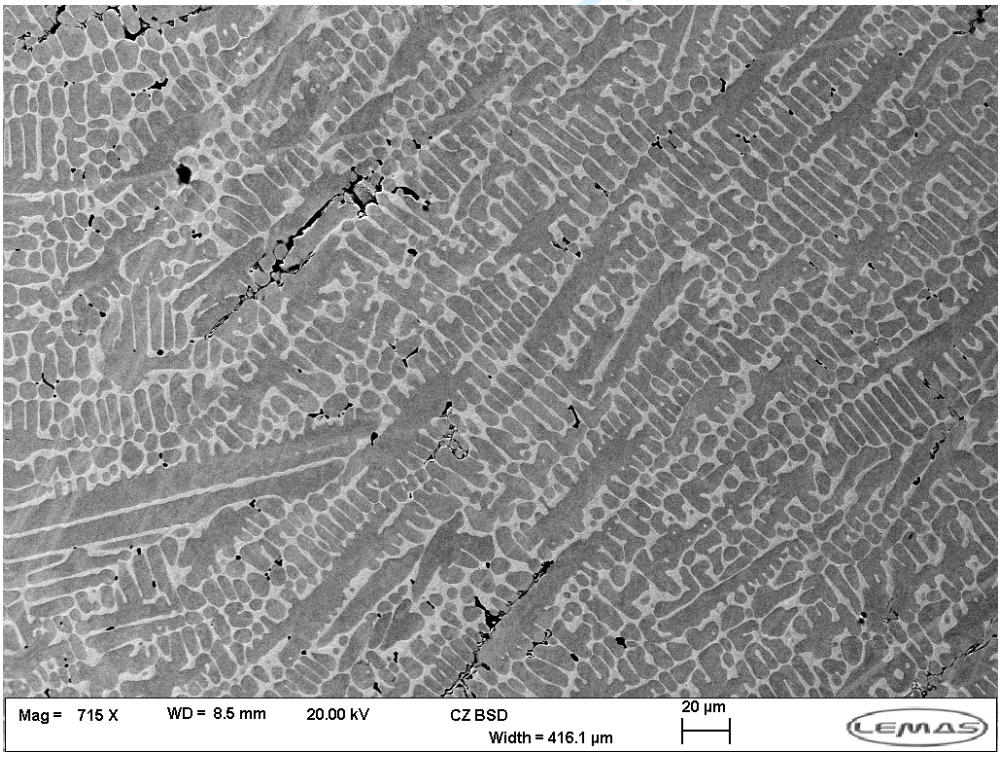

Fig. 3. Back scattered SEM image of arc melted Cu – 68.5 at. % Co alloy.

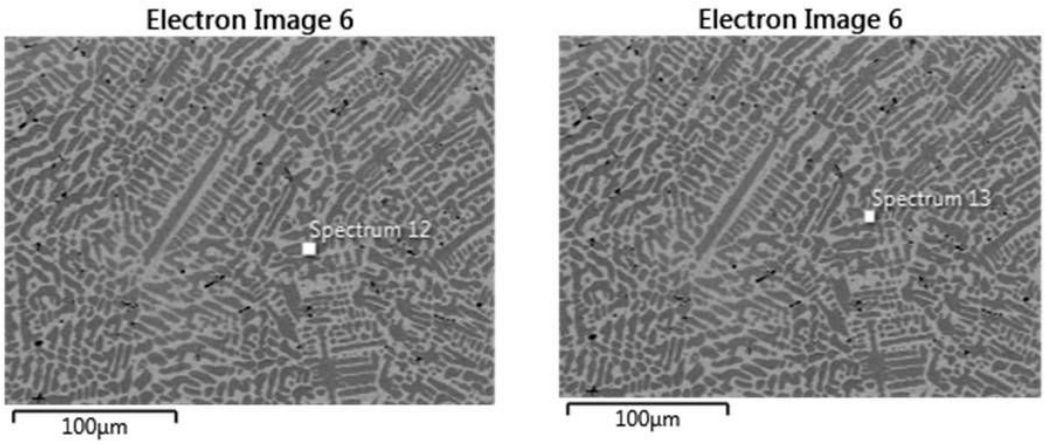

Element	At. %	
	Spectrum 12	Spectrum 13
Co	80.68	85.86
Cu	19.32	14.14

Fig. 4. EDS reading of dendrites in arc melted Cu – 68.5 at. % Co alloy.

Microstructures of the drop tube samples supports the metastable phase diagram estimates with evidence of liquid phase separation via binodal decomposition observed. The microstructures in the drop tube samples were of two major categories i.e. phase separated structures and non-phase separated structures. The phase separated structures had embedded dispersed spherical particles which were either copper or cobalt rich. Evidence of spinodal decomposition was not observed in any of the microstructures of this composition. Morphology of the non- phase separated structures were all dendritic. Fig. 5 shows some of the phase separated structures observed in the drop tube powders.

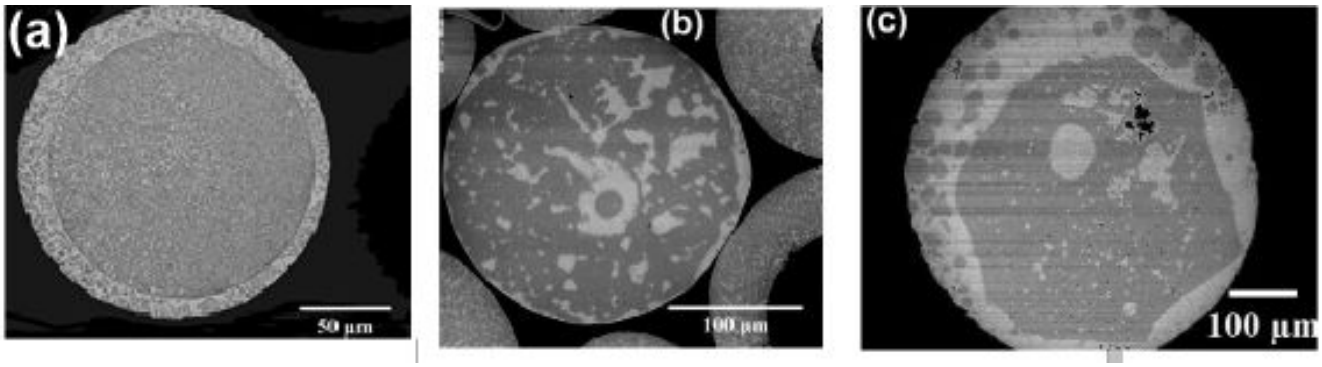

Fig. 5. Phase separated structures in undercooled drop tube powders of Cu 68.5 at. % Co alloy: (a) core shell type structure, (b) and (c) are evolving core shell type structures at different stages along its formation process. The dark phase is Co-rich while the light phase is Cu-rich.

Clearly, because of the compositional difference between the alloy in this research and that studied by Cao et al. [1], the liquidus temperature and undercooling is expected to vary. Their obtained liquidus temperature should and was lesser than that of the Cu – 68.5 at. % Co alloy. However, on the basis that a non-symmetrical miscibility gap exists in the system, their estimated critical undercooling was too high as binodal decomposition should occur in the alloy at much lesser undercooling. Their calculated miscibility gap places the liquidus temperature of the Cu – 68.5 at. % Co alloy at 1632 K with critical undercooling of 28 K to access the binodal region while that of the spinodal is placed as 67 K. Their estimated undercooling value of 263 K places their alloy as well as the one in this research well within the spinodal region. This seems to suggest that the higher the undercooling, the higher the liquidus temperature which is reasonable due to the fact that as the undercooling increases, the composition of the alloy is constantly changing with the Co – rich phase becoming more enriched. However, there is no microstructural evidence to suggest that this alloy spinodally decomposed.

Fig. 6 shows the first cycle DTA curves of the arc melted sample. Two strong endothermic peaks were prominent with onset temperatures of 1373 K and 1664 K. Since no metastable liquid phase separated structures were observed in its microstructure in Fig. 7, the equilibrium phase diagram

is used for analysis. The first onset temperature when traced on the phase diagram falls slightly above the T_p of the alloy system (1367 K) the second onset temperature is assumed to be the liquidus temperature of the alloy since it lies exactly on the liquidus line. However, the peak of this second event was observed at 1669 K and this we attribute to the latent heat of fusion. At 1599 K, a very strong exothermic event occurred with an onset temperature of 1636 K which falls slightly below the liquidus. On the equilibrium phase diagram, the alloy at this temperature is in the L + α region with liquid phase volume fraction of 56.72 % and composition of 81.66 at. % Co. The second exothermic event with onset temperature of 1375 K corresponds to the solidification of the Cu – rich inter dendritic space.

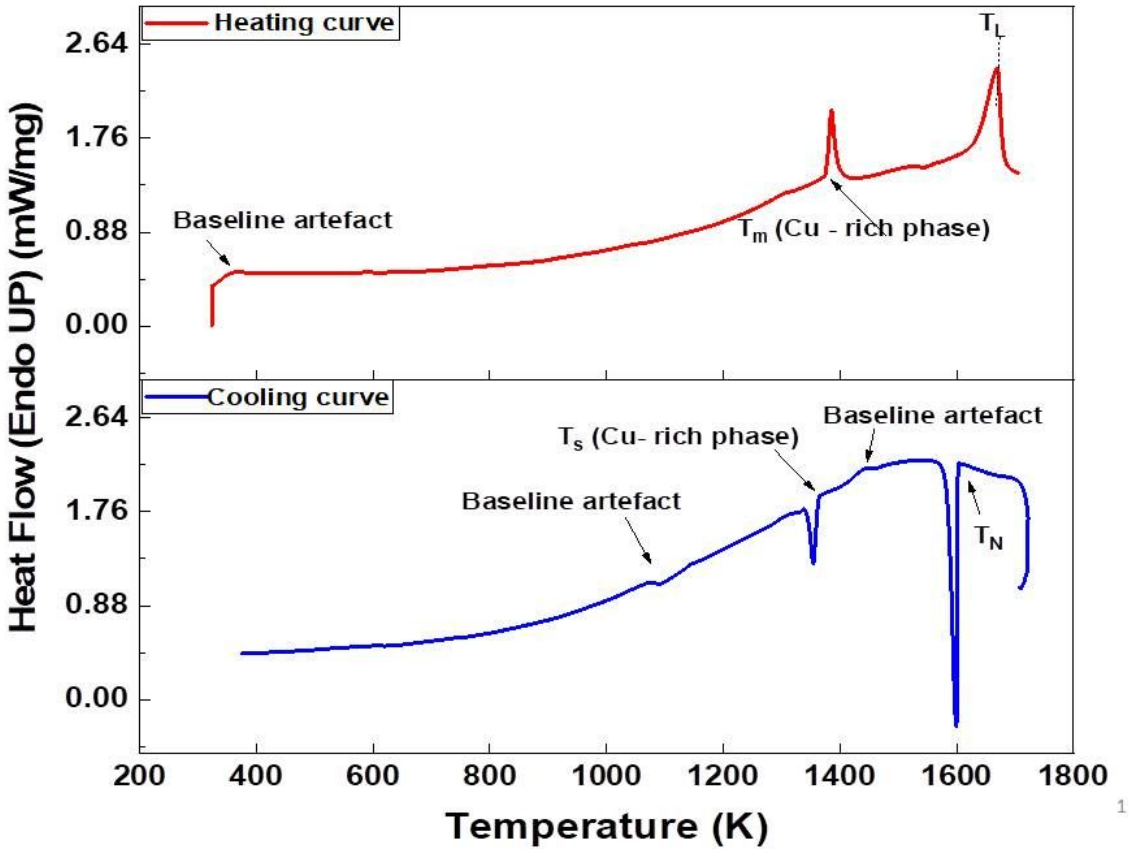

Fig. 6. First cycle DTA curves of arc melted Cu – 68.5 at. % Co alloy showing the T_m of the Cu – rich phase and T_N of α – Co dendrites.

The first endothermic event is thought to be the melting temperature (T_m) of the Cu – rich phase as the composition at this temperature when traced on the equilibrium phase diagram is majorly copper. The T_m of pure copper is 1358 K while that of pure cobalt is 1768 K. The prominent peak of the exothermic event observed at 1599 K is likely due to the formation of α – Co hence its onset temperature is taken as its nucleation temperature (T_N) in the alloy. This is confirmed by the microstructural image in Fig. 7 showing the presence of α – Co dendrites in the DTA sample and EDS gave their average composition as 82.2 at. % Co which is not far off from the composition of its starting material in Fig. 4.

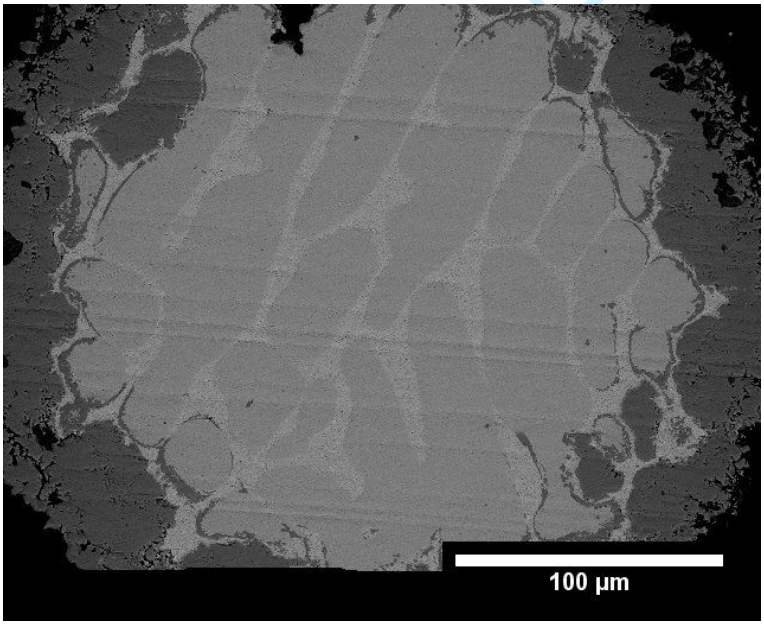

Fig. 7. Back scattered SEM image showing DTA processed sample of arc melted Cu – 68.5 at. % Co alloy.

In Fig. 8, the same events were observed on the curves of the first heating cycle of the larger drop tube powders (850^+ µm). However, the peaks were observed to be slightly displaced, for

instance, T_m was 1372 K in this sample compared to 1373 K observed in the arc melt sample. The second endothermic peak onset was at 1632 K. It is worth mentioning that a baseline artifact observed at 1090 K in the arc melt sample shifted to 1098 K in this drop tube powder size range and the feature is noticed to be considerably wider in this sample.

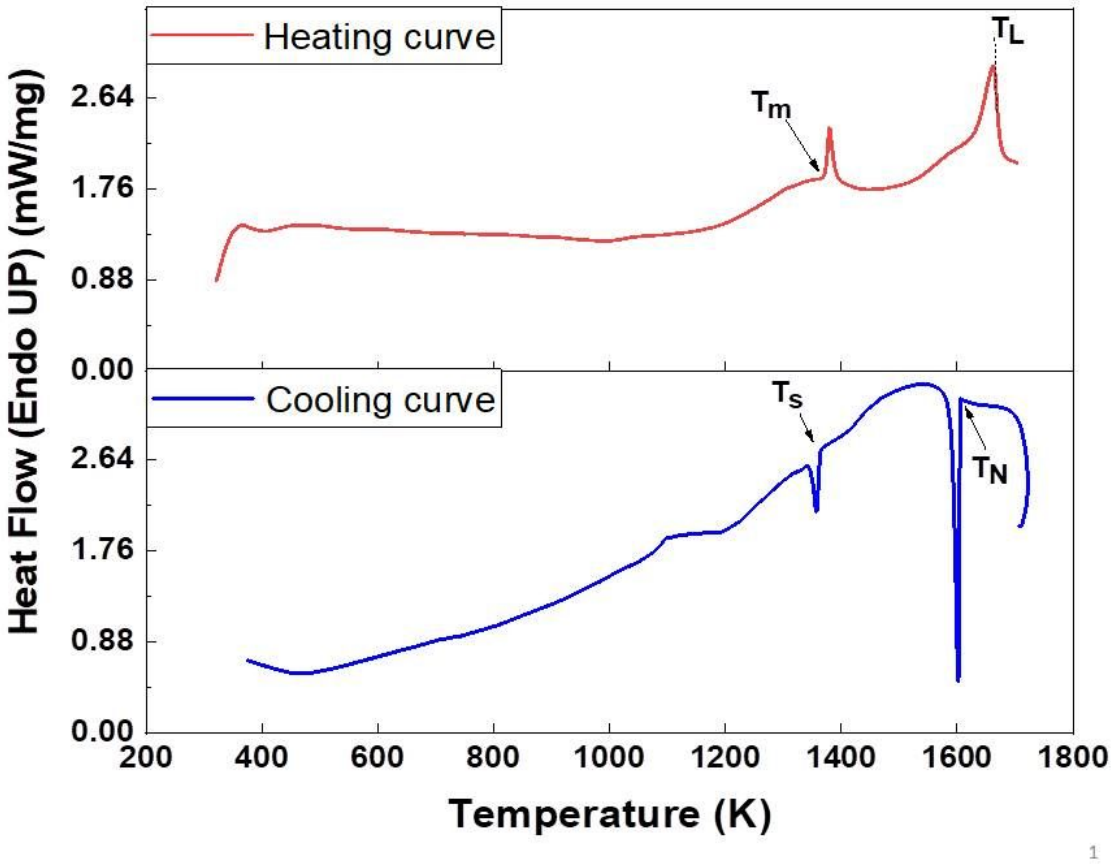

Fig. 8. DTA curves of the 850$^+$ µm drop tube powder of Cu – 68.5 at. % Co alloy showing T_m of the Cu – rich phase and T_N of α – Co dendrites.

In Fig. 9, the DTA curves in the drop tube powder in the < 38 µm sieve size fraction had four endothermic and exothermic events. The first endothermic event observed corresponding to the melting point in this powder (1375 K) differs by 2 K and 3 K to the arc melt sample and powder in the 850$^+$ µm size range respectively. At temperatures 1443 K and 1484 K the second and third

endothermic events occurred respectively as two small departures from the baseline; indicating that some sort of weak reactions occurred at these temperatures. When traced on the metastable phase diagram, the temperature 1443 K coincides with the binodal and spinodal curves but due to the estimated high undercooling necessary for the alloy to cool into the spinodal region, it is unlikely the alloy spinodally decomposed during the DTA experiment. However, when traced on the equilibrium phase diagram it hits the liquidus line and falls within the L + α – Co region with the volume fraction of the α – Co phase placed at 33 % while the liquid found to be Cu – rich had a composition of 40 at. % Co. The final endothermic event which was characterized by a broad peak had an onset temperature of 1542 K. The first exothermic event in this alloy powder size range occurred as a small departure from the baseline at 1176 K. The onset temperatures of the first, second and third exothermic peaks were 1620 K, 1616 K and 1373 K respectively.

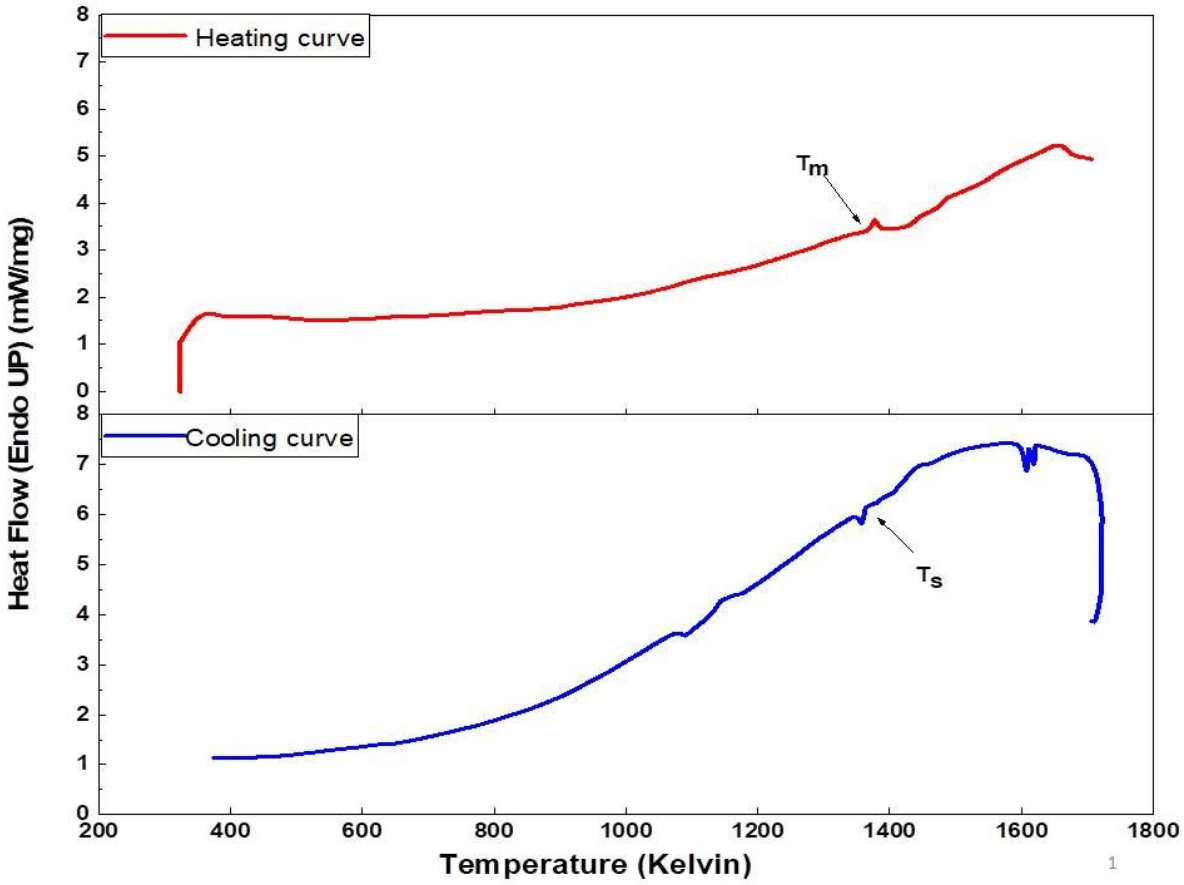

Fig. 9. DTA curves of the < 38 µm drop tube powder of the Cu – 68.5 at. % Co alloy.

Two transformations known to occur at lower temperatures on the equilibrium phase diagram of the Co – Cu system are the magnetic transformation at 1323 K and eutectoid transformation at 695 K. It is difficult to conclude if the baseline event observed in the larger drop tube powder is an artifact or a feature of the alloy; however, it is thought that the temperature of the event corresponds to the magnetic transformation temperature which has been known to be lowered with increasing Cu content. If this were the case, the alloy most probably crossed the T_p line and the use of the equilibrium phase diagram in this analysis rather than the metastable one is justified. Although the first exothermic event in the smaller powder also occurred as a small

departure from the baseline, the energy observed to be associated with the event was rather low (-1.33 J/g).

In the 850^{+} μm powder, the peak positions on the heating curve and second peak of the cooling curve are exactly **3 K** lesser than that of the arc melt sample while the first peak on the cooling curve differs from that of the arc melt sample by **2 K**. However, the first exothermic event on the cooling curve in this powder sample has an onset temperature (which coincides with the temperature at which α – Co starts to nucleate) that is higher than the arc melt sample (1608 K). The second exothermic events on the equilibrium phase diagram coincides with temperature at which the Cu – rich phase starts to solidify (T_s). Therefore the microstructure is expected to be α -Co dendrites with Cu – rich inter dendritic space. This is confirmed by the microstructure in Fig. 10.

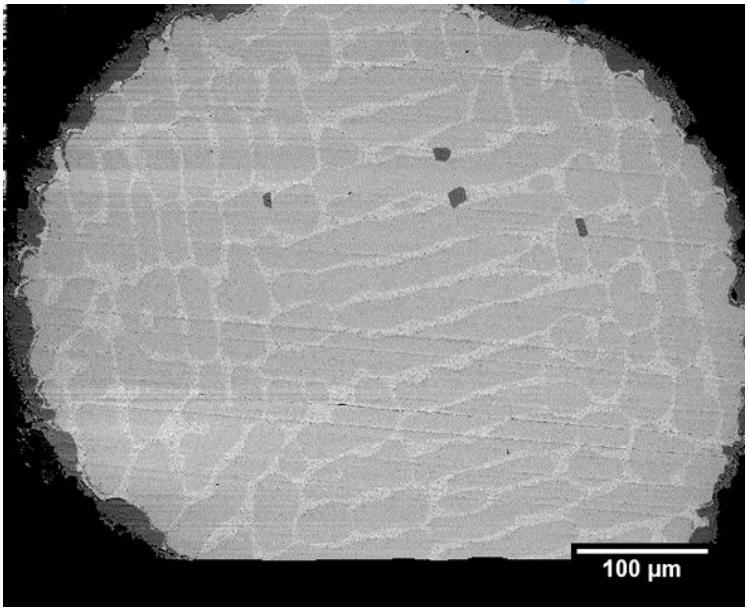

Fig. 10. Back scattered SEM image of DTA processed sample of 850^{+} μm drop tube powder of the Cu – 68.5 at. % Co alloy.

The presence of a third exothermic peak on the DTA cooling curve of the < 38 μm powder sample is initially thought to be due to LPS based on what looked like spherical structures on its microstructure in Fig. 11. Evidently, the microstructure shows what looks like spherical particles but upon tracing out the temperatures on the metastable phase diagram, these coincide with the spinodal line. Since there is no evidence of spinodal decomposition in this microstructure and other microstructures of the alloy, the use of the equilibrium phase diagram in analysing it is justified. It is therefore concluded that the spherical particles are dendrite tips.

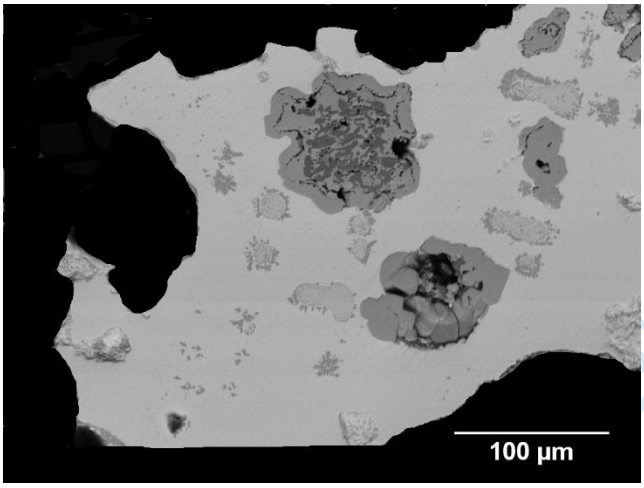

Fig.11. Back scattered SEM image of DTA sample of the < 38 μm drop tube powder of the Cu – 68.5 at. % Co alloy.

Conclusion

In conclusion, analysis of the onset temperature of the events on the DTA curves on the phase diagram of the system shows that as the powder size decreased, volume fraction of the α – Co phase increased. This is reflected by the variation of the T_m as sample size decreased; a departure from the melting temperature of pure copper was observed. The implication of this is that as undercooling increased (higher undercooling in smaller powder droplets), the copper content gradually reduces.

Acknowledgement

Oluwatoyin Jegede is a commonwealth scholar, sponsored by the UK government.

Competing interest statement

The authors declare there are no competing interests.

Author contribution statement

All authors actively contributed towards the writing of the manuscript and have given approval to its final version.

References

(1) Cao, C.; Letzig, T.; Görler, G..; Herlach, D. *J. Alloys Compd.* **2001**, *325* (1–2), 113.

(2) Munitz, A.; Abbaschian, R. *Metall. Mater. Trans. A* **1996**, *27* (12), 4049. doi.org/10.1007/BF02595654.

(3) Yamauchi, I.; Ueno, N.; Shimaoka, M.; Ohnaka, I. *J. Mater. Sci.* **1998**, *33* (2), 371. doi.org/10.1023/A:1004319829612.

(4) Munitz, A.; Abbaschian, R. *J. Mater. Sci.* **1991**, *26* (23), 6458. doi.org/10.1007/BF00551897.

(5) Jegede, O. E.; Cochrane, R. F.; Mullis, A. M. *J. Mater. Sci.* **2018**, *53* (16), 11749. doi.org/10.1007/s10853-018-2417-y.

(6) Cao, C.; Görler, G.; Herlach, D.; Wei, B. *Mater. Sci. Eng. A* **2002**, *325* (1–2), 503. doi.org/10.1016/S0921-5093(01)01756-7.

(7) Nakagawa, Y. *Acta Metall.* **1958**, *6* (11), 704. doi.org/10.1016/0001-6160(58)90061-0.

(8) Robinson, M. B.; Li, D.; Rathz, T. J.; Williams, G. *J. Mater. Sci.* **1999**, *34* (15), 3747. doi.org/10.1023/A:1004688313591.

(9) Palumbo, M.; Curiotto, S.; Battezzati, L. *Calphad* **2006**, *30* (2), 171. doi.org/10.1016/J.CALPHAD.2005.10.007.

(10) Zhang, Y.; Gao, J.; Yasuda, H.; Kolbe, M.; Wilde, G. *Scr. Mater.* **2014**, *82*, 5. doi.org/10.1016/j.scriptamat.2014.03.003.

(11) Cao, C.; Wang, N.; Wei, B. *Sci. China Ser. A Math.* **2000**, *43* (12), 1318. doi.org/10.1007/BF02880070.

(12) Luo, X.; Chen, L. *Sci. China Ser. E Technol. Sci.* **2008**, *51* (9), 1370. doi.org/10.1007/s11431-008-0128-3.

(13) Zhang, Y. K.; Gao, J.; Nagamatsu, D.; Fukuda, T.; Yasuda, H.; Kolbe, M.; He, J. C. *Scr. Mater.* **2008**, *59* (9), 1002. doi.org/10.1016/j.scriptamat.2008.07.005.

(14) Zhang, Y.; Gao, J.; Wei, L.; Kolbe, M.; Volkmann, T.; Herlach, D. *J. Mater. Sci.* **2011**, *46* (20), 6603.

(15) Kolbe, M.; Gao, J. R. *Mater. Sci. Eng. A* **2005**, *413–414*, 509. doi.org/10.1016/j.msea.2005.08.170.

(16) Cao, C. D.; Wei, B.; Herlach, D. M. *J. Mater. Sci. Lett.* **2002**, *21* (41), 341. doi.org/10.1023/A:1017913029777.

(17) Mullis, A. M.; Jegede, O. E.; Bigg, T. D.; Cochrane, R. F. *Acta Mater.* **2020**, *188*, 591. doi.org/10.1016/j.actamat.2020.02.017.

(18) Zhai, W.; Wei, B. *J. Chem. Thermodyn.* **2015**, *86*, 57. dx.doi.org/10.1016/j.jct.2015.02.021.

(19) Erol, M.; Böyük, U.; Volkmann, T.; Herlach, D. *J. Alloys Compd.* **2013**, *575*, 96.

(20) Jegede, O. E.; Haque, N.; Mullis, A. M.; Cochrane, R. F. *Can. J. Chem.* **2021**. doi.org/10.1139/cjc-2021-0064.

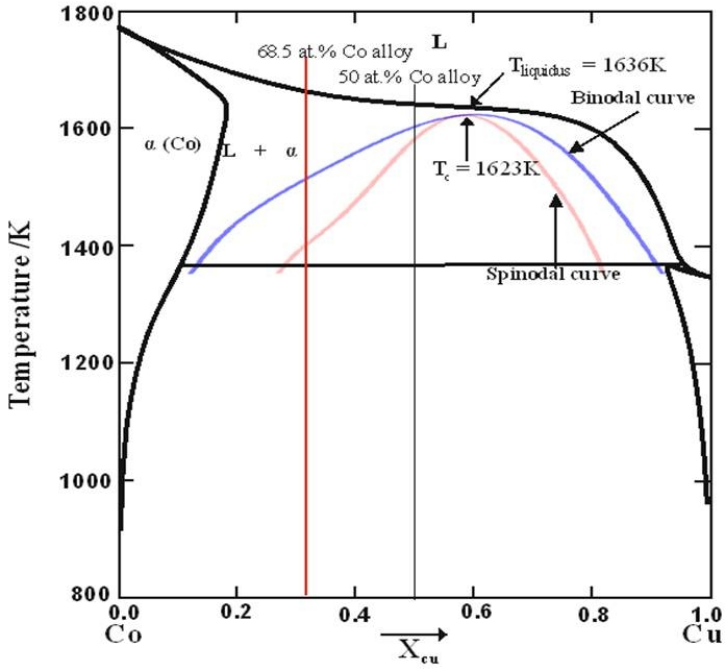

Fig. 1. Metastable phase diagram of the Cu-Co alloy system with calculated miscibility gap showing the binodal and spinodal curves. The solidification path of the Cu 68.5 at. % Co alloy and that of alloy of equi – atomic composition is indicated by the red and black lines respectively 5.

254x190mm (96 x 96 DPI)

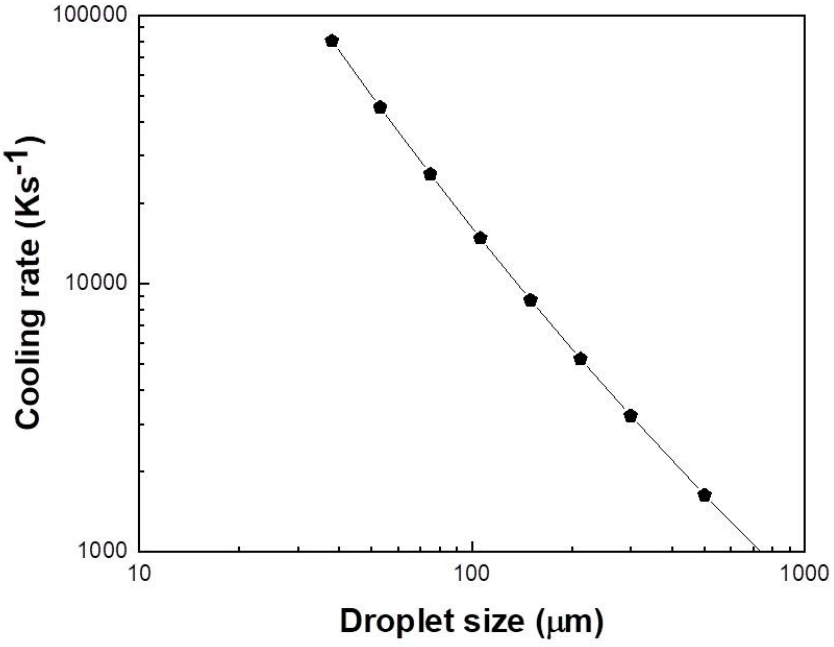

Fig. 2. Estimated cooling rate as a function of droplet diameter in Cu – 68.5 at. % Co alloy.

254x190mm (96 x 96 DPI)

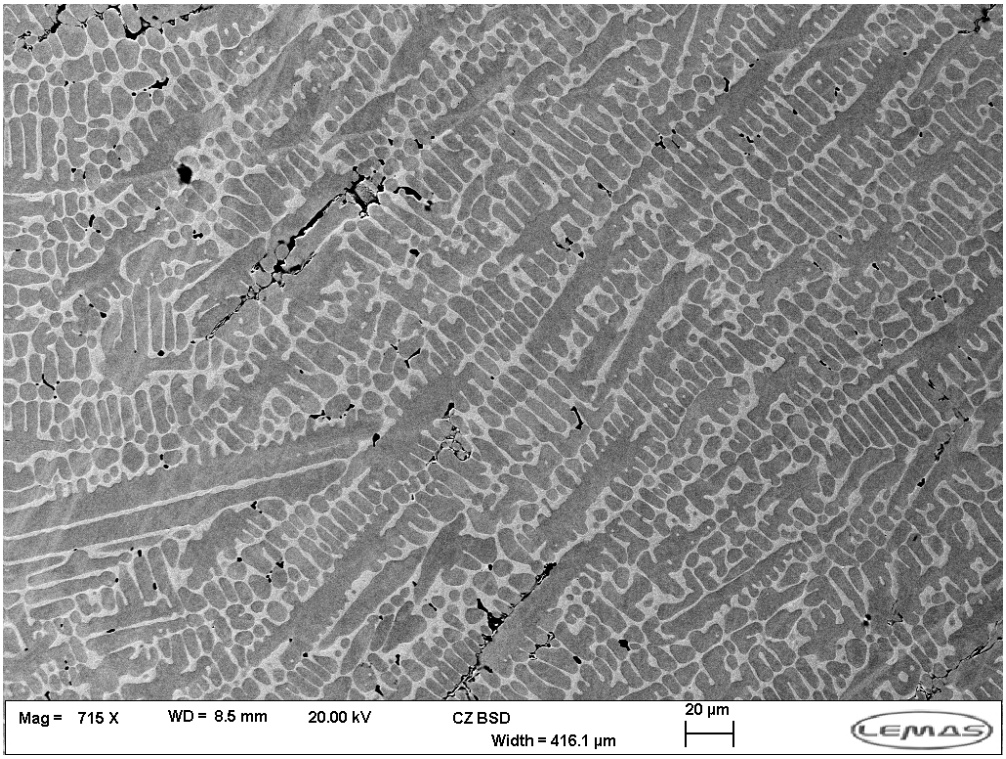

Fig. 3. Back scattered SEM image of arc melted Cu – 68.5 at. % Co alloy.

26009x19507mm (1 x 1 DPI)

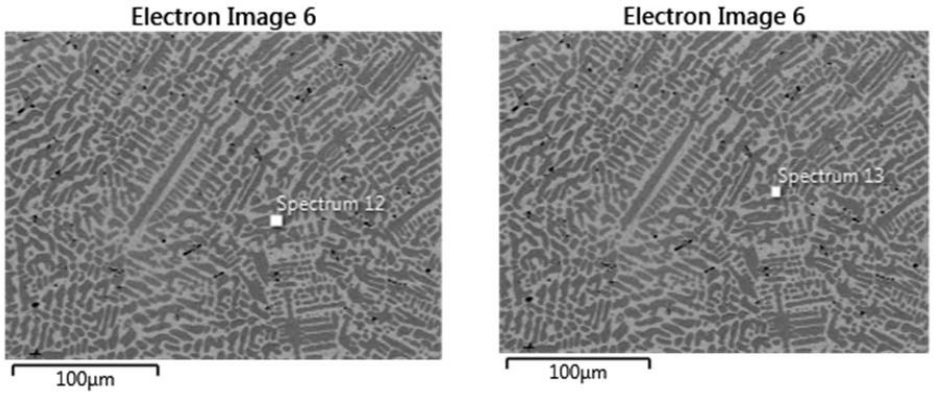

Element	At. %	
	Spectrum 12	Spectrum 13
Co	80.68	85.86
Cu	19.32	14.14

Fig. 4. EDS reading of dendrites in arc melted Cu – 68.5 at. % Co alloy.

254x190mm (96 x 96 DPI)

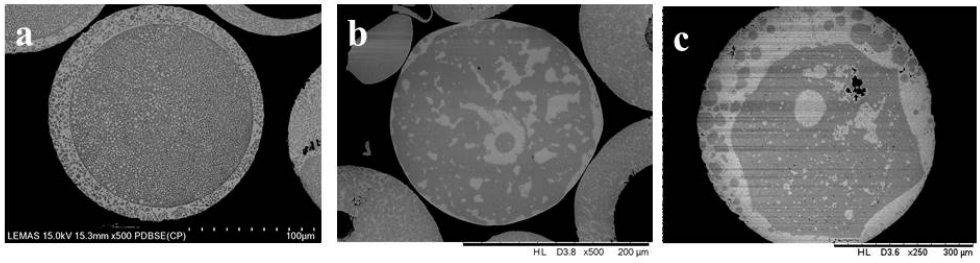

Fig. 5. Phase separated structures in undercooled drop tube powders of Cu 68.5 at. % Co alloy: (a) core shell type structure, (b) and (c) are evolving core shell type structures at different stages along its formation process. The dark phase is Co-rich while the light phase is Cu-rich.

254x190mm (96 x 96 DPI)

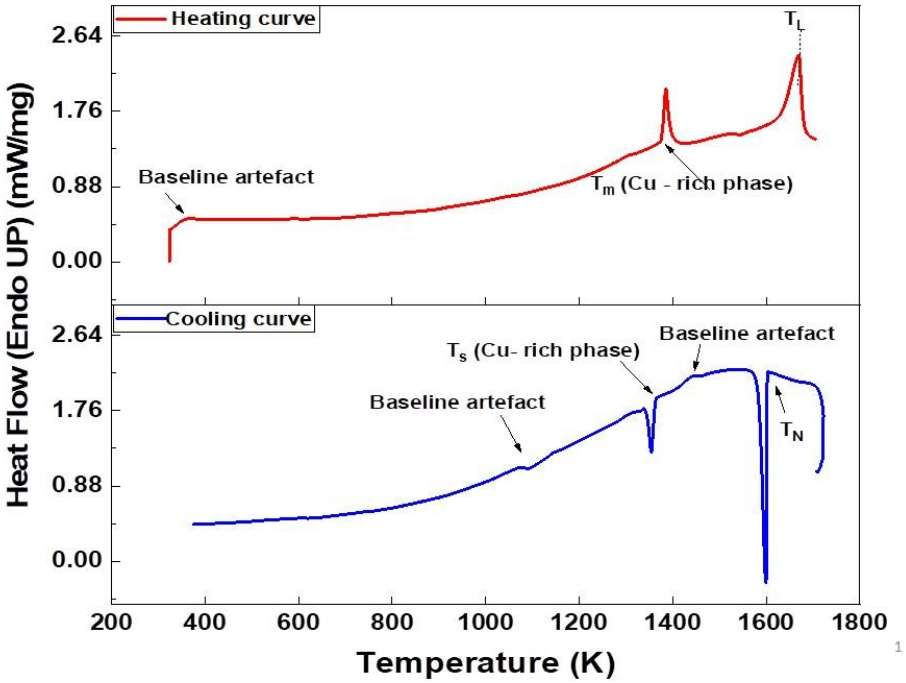

Fig. 6. First cycle DTA curves of arc melted Cu – 68.5 at. % Co alloy showing the Tm of the Cu – rich phase and TN of α – Co dendrites.

254x190mm (96 x 96 DPI)

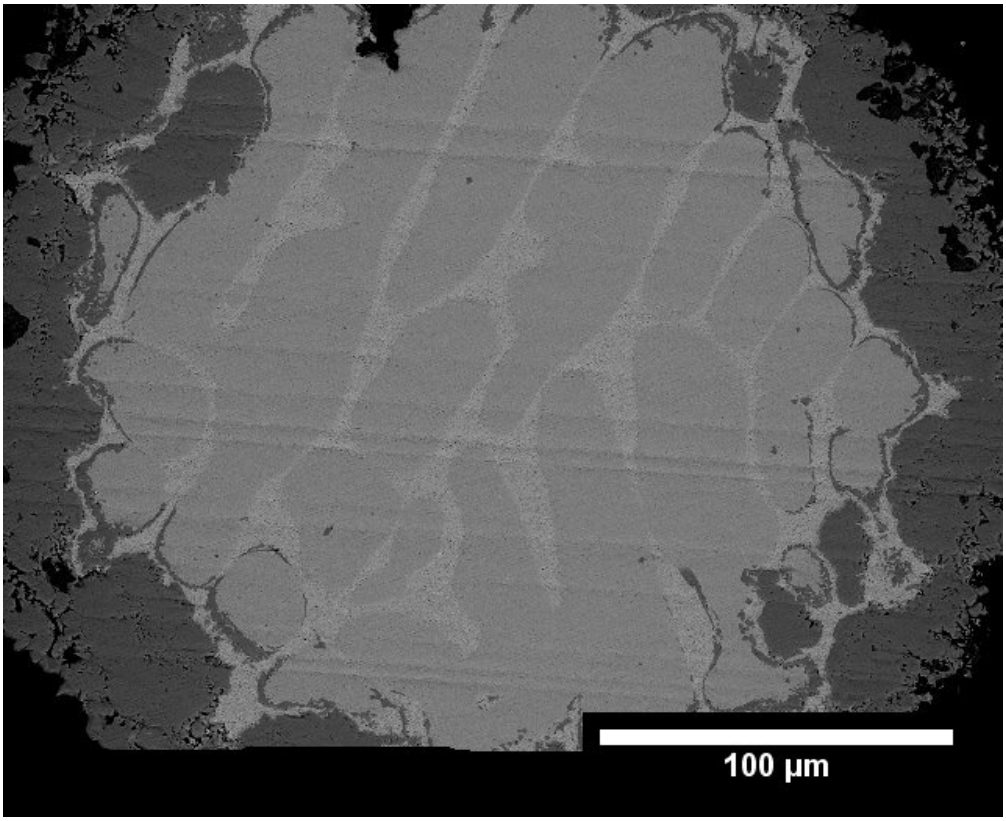

Fig. 7. Back scattered SEM image showing DTA processed sample of arc melted Cu – 68.5 at. % Co alloy.

225x183mm (72 x 72 DPI)

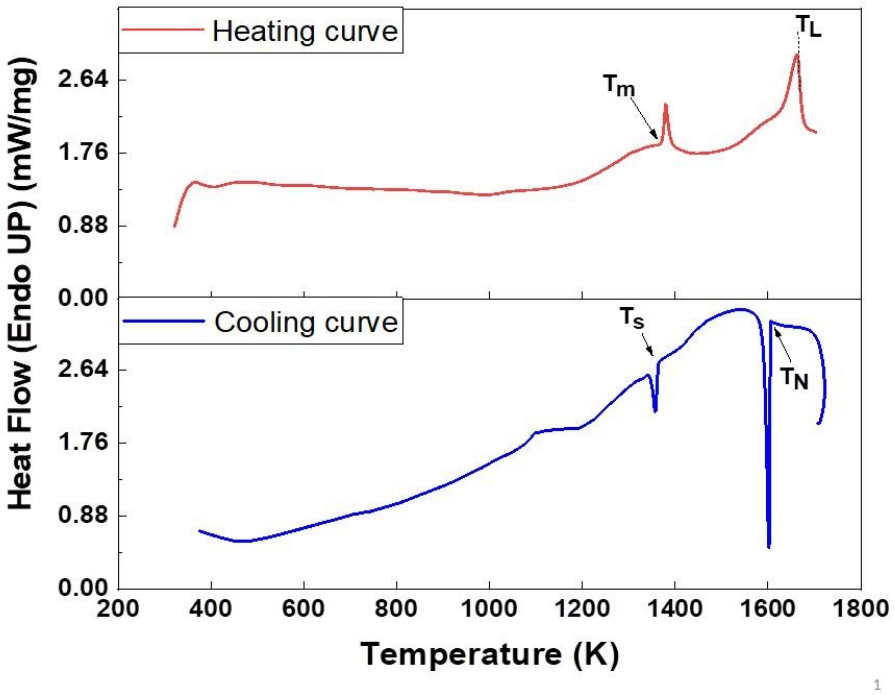

Fig. 8. DTA curves of the 850+ μm drop tube powder of Cu – 68.5 at. % Co alloy showing Tm of the Cu – rich phase and TN of α – Co dendrites.

254x190mm (96 x 96 DPI)

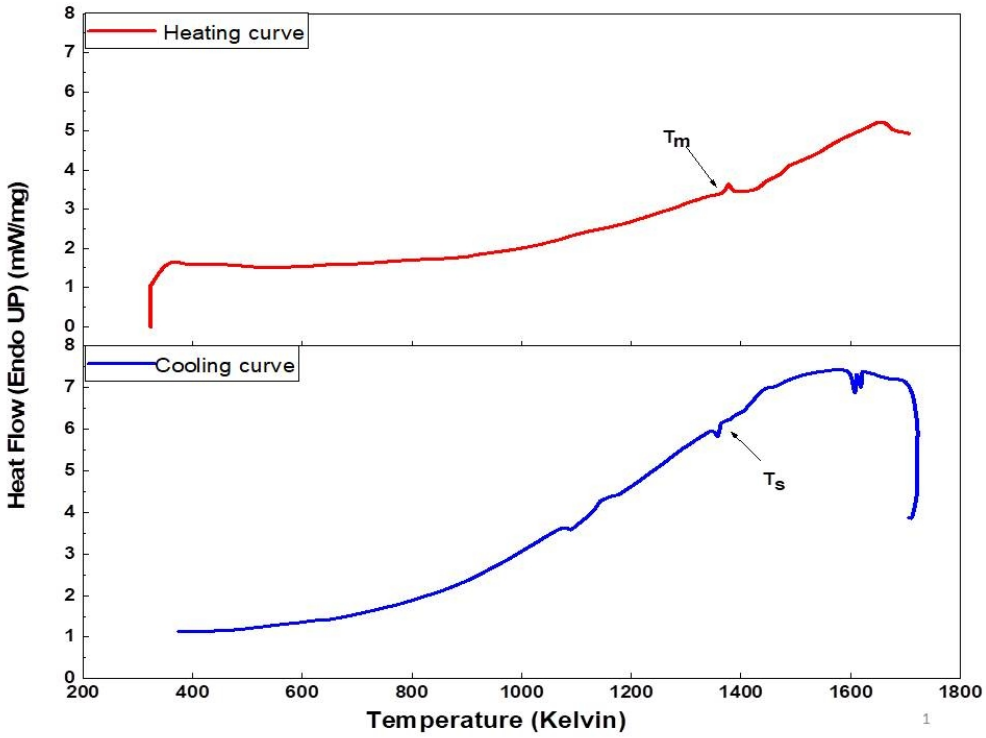

Fig. 9. DTA curves of the < 38 μm drop tube powder of the Cu – 68.5 at. % Co alloy.

254x190mm (96 x 96 DPI)

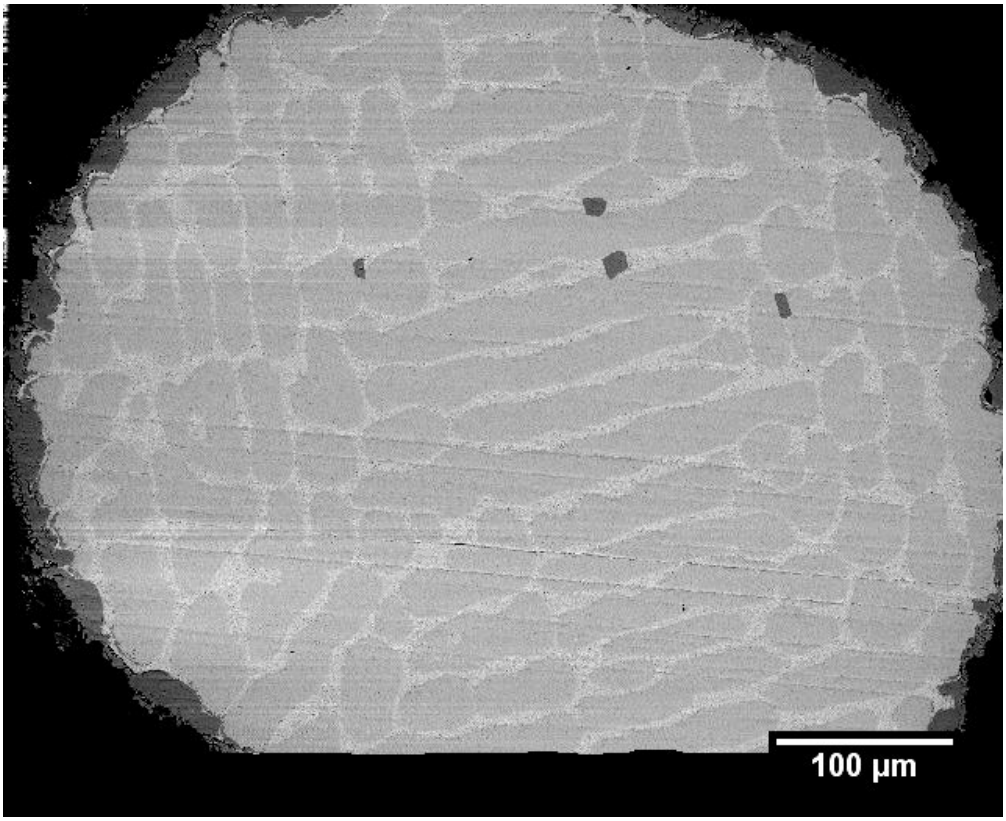

Fig. 10. Back scattered SEM image of DTA processed sample of 850+ µm drop tube powder of the Cu – 68.5 at. % Co alloy.

225x183mm (72 x 72 DPI)

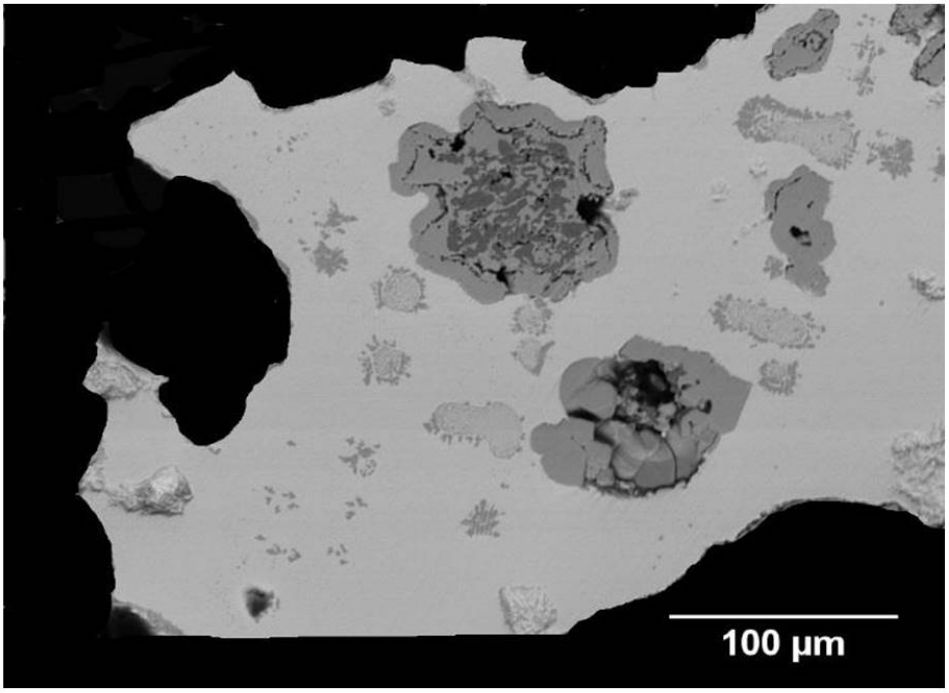

Fig.11. Back scattered SEM image of DTA sample of the < 38 µm drop tube powder of the Cu – 68.5 at. % Co alloy.

254x190mm (96 x 96 DPI)